Numerical simulation of the overpressure at Martel facility: combustion and wave generation

Baptiste Jouy and Julien Troyes
ONERA, Châtillon, France

Jean-Baptiste Dargaud
ONERA, Châtillon, France, CNES Evry, France

And

François Vuillot
ONERA, Châtillon, France

Abstract

Space vehicles are submitted to severe conditions during lift-off due to overpressure wave, a phenomenon which has been thoroughly studied over the years by CNES, Onera and Astrium-ST. Among the test centers used, the Martel facility allows repeatable pressure wave generations. This study focuses on the numerical simulation of the overpressure generation at the Martel facility.
After an initial combustion computation which was aimed at defining the required initial conditions, the overpressure simulation results proved to be in good agreement with the experimental sensor histories and were used in order to perform an accurate description of the overpressure wave generation at Martel.

1. Introduction

During lift-off, a space launcher is submitted to harsh conditions and severe loads are transmitted to its structure. Those loads are caused by a phenomenon called overpressure wave, which is generated at the ignition of Solid Rocket Motors (SRM) boosters [1]. The topic has been thoroughly studied for several years by CNES, Onera and Astrium-ST, in the framework of the AEID program, a R&T CNES funding which was able to define several key factors in the overpressure wave generation, such as the combustion chamber pressure rise rate. The program relied first on subscale model SRM firings at the Onera Fauga-Mauzac center [2], and then on series of blast tests at the Martel facility, developed by CNES and operated by CEAT in Poitiers [3][4]. More recently, overpressure wave numerical simulations were carried out using CEDRE code [5][6][7], an unsteady reactive LES code developed by Onera [8]. The present paper will focus on the numerical simulation of the overpressure recorded during a Martel experiment, which was carried out in two steps:

- a combustion computation aimed at defining the required initial conditions,
- the main pressure wave computation.

Finally, results will be discussed in the last part and compared to experimental results.

2. Experiments carried out at Martel test facility

2.1 Pressure wave generator

Figure 1: View of the pressure wave generator at Martel facility

The Martel facility (Figure 1) was developed in the framework of the research program AEID. Originally aimed at studying and reducing launch vehicle noise induced at lift-off, the facility was equipped in 2008 with a system able to simulate the overpressure wave phenomenon [3]. This blast generator (composed of a spherical tank, a diaphragm with a remote-controlled striker, a secondary chamber and a nozzle) allows less expensive series of reproducible experiments than scaled-down SRM tests which were previously fired [2].

Several experimental campaigns have been carried out since its implementation, first with the gas generator only, then with a reduced scale flame trench similar to the Ariane 5 one at the Kourou launchpad [4]. This particular case, as described on the Figure 2, will be studied in the article.

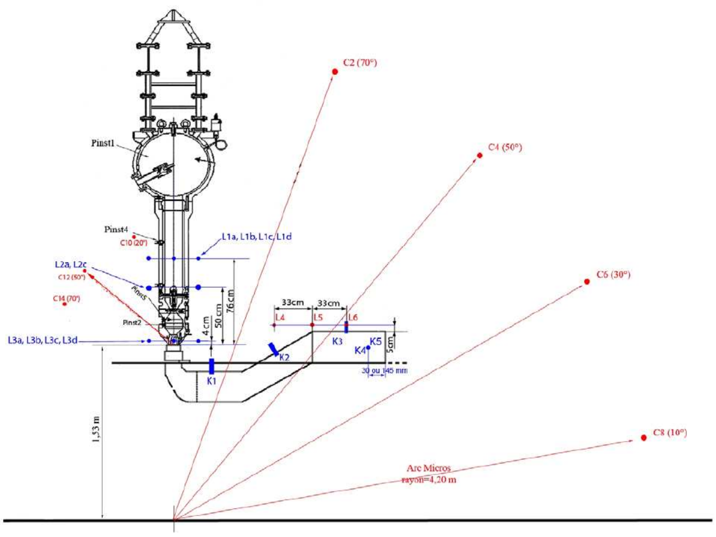

Figure 2: Diagram of the generator, the flame trench and their surrounding acoustics sensors

2.2 Experiment description

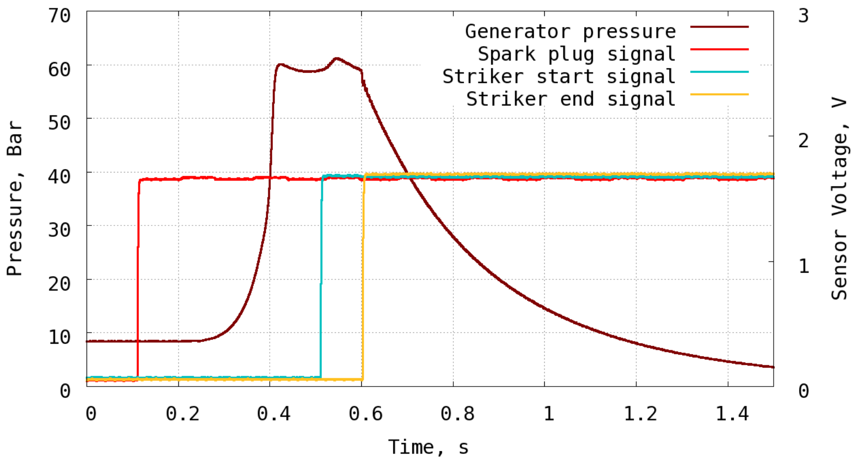

Figure 3: Timeline of the Martel experiment

A stoichiometric mixture of methane and air is injected in the generator at 8.5 bar. The temperature is regulated at 310 K. The ignition is triggered by a spark plug located at the center of the sphere. The pressure peaks at 60 bar, as displayed on Figure 3. The striker movement is initiated 400 ms after the ignition order, and breaks the diaphragm about 100 ms later.

The burnt gases flow through a nozzle into the secondary chamber that is quickly pressurized. The chamber volume mitigates the secondary chamber pressure rise rate, and therefore the resulting overpressure wave. The volume may vary from 2 to 9 l, and this study focuses on a 3.5 l chamber. The gases finally exhaust from the chamber through a second nozzle. At this point, the overpressure wave may simultaneously:

- propagate into open space and reflect on the structure, hence denominated *Ignition OverPressure* (IOP).
- enter the flame trench and be reemitted at its exit, thus called *Duct OverPressure* (DOP).

Several acoustic transducers around the generator record the pressure histories during the blast (cf Figure 2). Sensors L1a to L3d (Figure 2, blue) are located near the generator and focus on the loads transmitted to the generator structure, whereas transducers L4 to L6 (Figure 2, red) underline the propagation of the *Duct OverPressure* from the trench exit to the generator. Finally, arcs of sensors C10 to C14 and C2 to C8 (Figure 2, red) highlight the directivity of the *Ignition OverPressure* and the *Duct OverPressure*, respectively. These arrays of sensors lead to an exhaustive description of the overpressure waves, which allows accurate comparisons between the experiment and the computation.

3. Combustion computation

During the blast, the experimental temperature and the final composition of the burnt mixture are unknown. As they are key conditions of the pressure wave computation, they have to be estimated using a reactive LES simulation of the combustion occurring inside the generator.

3.1 Configuration

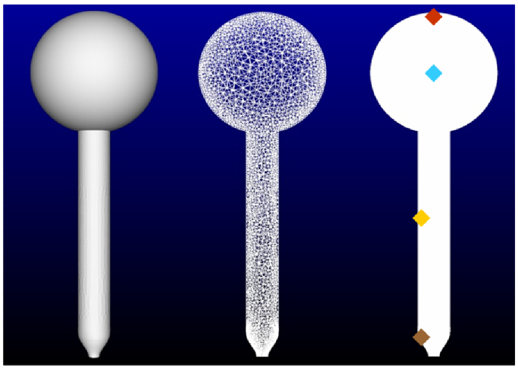

Figure 4: From left to right: geometry, mesh, and location of the numerical pressure transducers (from top to bottom, G1 to G4)

The global geometry is edited in order to keep only the primary chamber, which leads to a 60,000 tetraedron mesh created using the Centaur grid software (cf Figure 4). All the boundary conditions, including the diaphragm, are solid walls in the computation.

Table 1: Species mass fraction table

CH_4	H_2O	CO	CO_2	O_2	N_2
0.05505	0	0	0	0.22018	0.72477

$$\begin{cases} CH_4 + \frac{3}{2}\,O_2 \rightarrow CO + 2\,H_2O \\ CO + \frac{1}{2}\,O_2 \leftrightarrow CO_2 \end{cases} \quad \textbf{(1)}$$

The reactants, CH_4 and air, are set in stoichiometric ratio, in an ideal mixture (cf Table 1). The kinetic scheme used in the computation is a two-step mechanism optimized for CFD codes [9], involving CH_4, O_2, CO, CO_2 and H_2O (1). The Smagorinsky subgrid scale model is activated.

The spatial discretization is provided by a second order scheme, numerical Euler fluxes are Roe fluxes. Time resolution is first order implicit and performed with a global time step of 5.10^{-6}s. Implicit linear system resolution is done by a GMRES method with block diagonal preconditioning. The Cp(T) coefficients of the reactants are modelled by 7th order polynomials. The first 100 ms of the combustion are computed on 32 cores of the Nehalem cluster of Onera, for an elapsed computation time of 6 hours.

3.2 Results

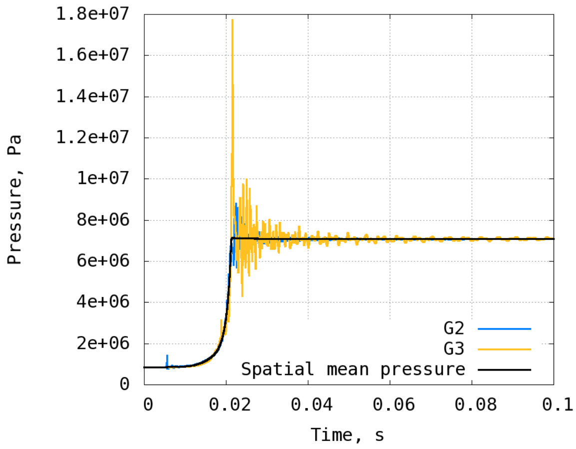

Figure 5: Evolution of the pressure in the generator

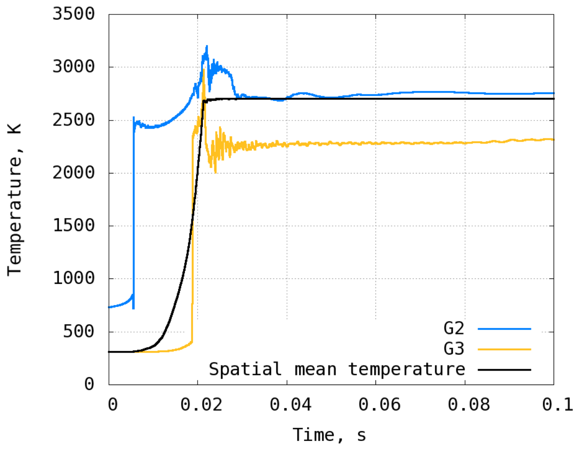

Figure 6: Evolution of the temperature in the generator

Figures 5 and 6 show that the combustion occurs in 50 ms, which can be compared to the 150 ms of the initial experimental combustion (cf Figure 3, 03-0.45 s). Those discrepancies in the combustion rate could be explained by an ideal mixture in the computation that favors a fast combustion. The influence of the kinetic scheme should not be ruled out either. Besides, a 400 K difference in the final temperature can be observed between G2 (center of the sphere, cyan) and G3 (center of the cylinder, yellow). That gap can be related to a slightly more complete combustion in the sphere than in the cylinder.

While the diaphragm is located at the bottom of the cylindrical tank, the sphere is connected at its top. During the first milliseconds of the blast, the only burnt gases escaping the generator come from the cylindrical part. The chemical and thermodynamical properties of the burnt gases used in the wave computation will therefore be determined on the cylindrical part of the generator, rather than averaged on the whole tank.

The pressure given by the combustion computation is higher than the Martel experimental pressure. The 10 bar gap might be linked to thermal losses on the generator walls. Other computations taking into account thermal losses on walls returned a 3.5 bar drop in the computed pressure, without influence on the computed temperature. As a result, the pressure used in the computation will be the experimental pressure (57.4 bar), while the temperature will be the computed temperature (2390 K).

4. Overpressure wave computation

4.1 Configuration

The global geometry – composed of the generator and the flame trench - is now refined and meshed in order to create a 12 million elements hybrid grid, using the Centaur software (Figure 7).

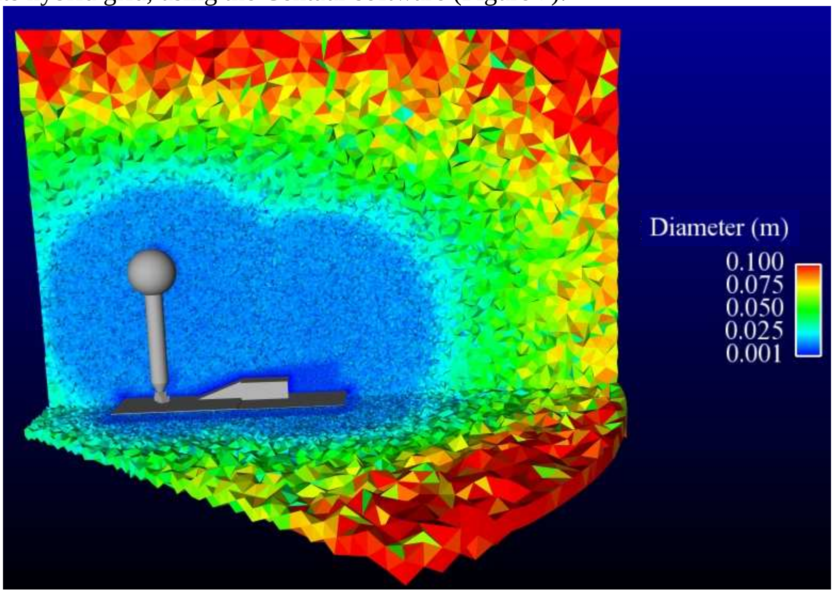

Figure 7: View of the generated mesh

The mesh is split in 4 domains (Figure 8) whose characteristics are given in Table 2. 3 layers of prisms are set at the nozzle exit and in the flame trench, the rest of the elements being tetraedrons. The elements are refined around the generator following two spheres of refinement, one centered on the nozzle exit and the other centered on the trench exit.

Table 2: Characteristics of the generated mesh

Domain	**Number of elements**	**Tetraedrons**	**Prisms**
Main domain	**11 450 107**	**11 424 155**	**24 646**
Primary chamber	**376 661**	**375 479**	**997**
Secondary chamber	**126 407**	**120 503**	**5 365**
Trench	**2 613 890**	**1 620 414**	**991 274**
Total	**14 567 065**	**13 540 551**	**1 022 282**

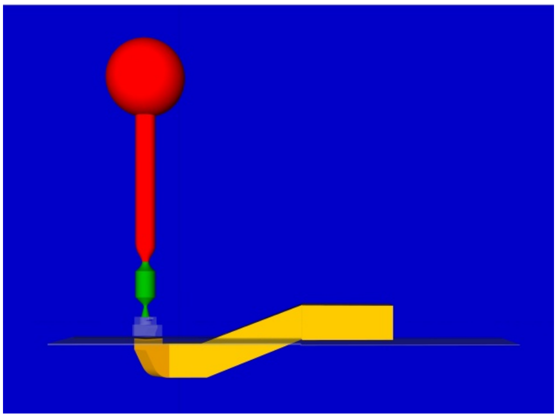

Figure 8: View of the different domains

In order to increase the computation speed, only 2 different species are used, *air* and *products*, created from a combination of the different burnt products measured in part 3 (cf Table 3). Their thermodynamic properties are deduced from their constituants. Table 3 details the initial conditions for each domain. While the primary chamber is initialized at the pressure and temperature and composition of the burnt gases, the other domains are set at the pressure and temperature measured during the experiment.

Table 3: Initial conditions of the pressure wave computation

Domains	Global species	Pressure (Pa)	Temperature (K)	Species	Mass fraction
Primary chamber	Products	5740000	2656.8	CO	0.010927
				CO_2	0.133782
				H_2O	0.123659
				O_2	0.006829
				N_2	0.724803
Secondary chamber	Air	100500	285	O_2	0.233000
				N_2	0.767000
Main domain	Air	100500	285	O_2	0.233000
				N_2	0.767000
Trench	Air	100500	285	O_2	0.233000
				N_2	0.767000

The boundary conditions are solid wall for the ground, the generator and the trench, and non-reflective for the other boundaries. The computation is non reactive unsteady LES, and is initiated on 128 cores of the Nehalem cluster of Onera, numerical parameters being similar to those used in part 3.

4.2 Sensor Results

The pressure histories of the Cedre computation are processed by a low pass filter using a cut-off frequency of 2 kHz, and are compared to the experimental reference (cf Figure 9). That reference was previously obtained averaging the 7 reference gusts generated at the Martel facility.

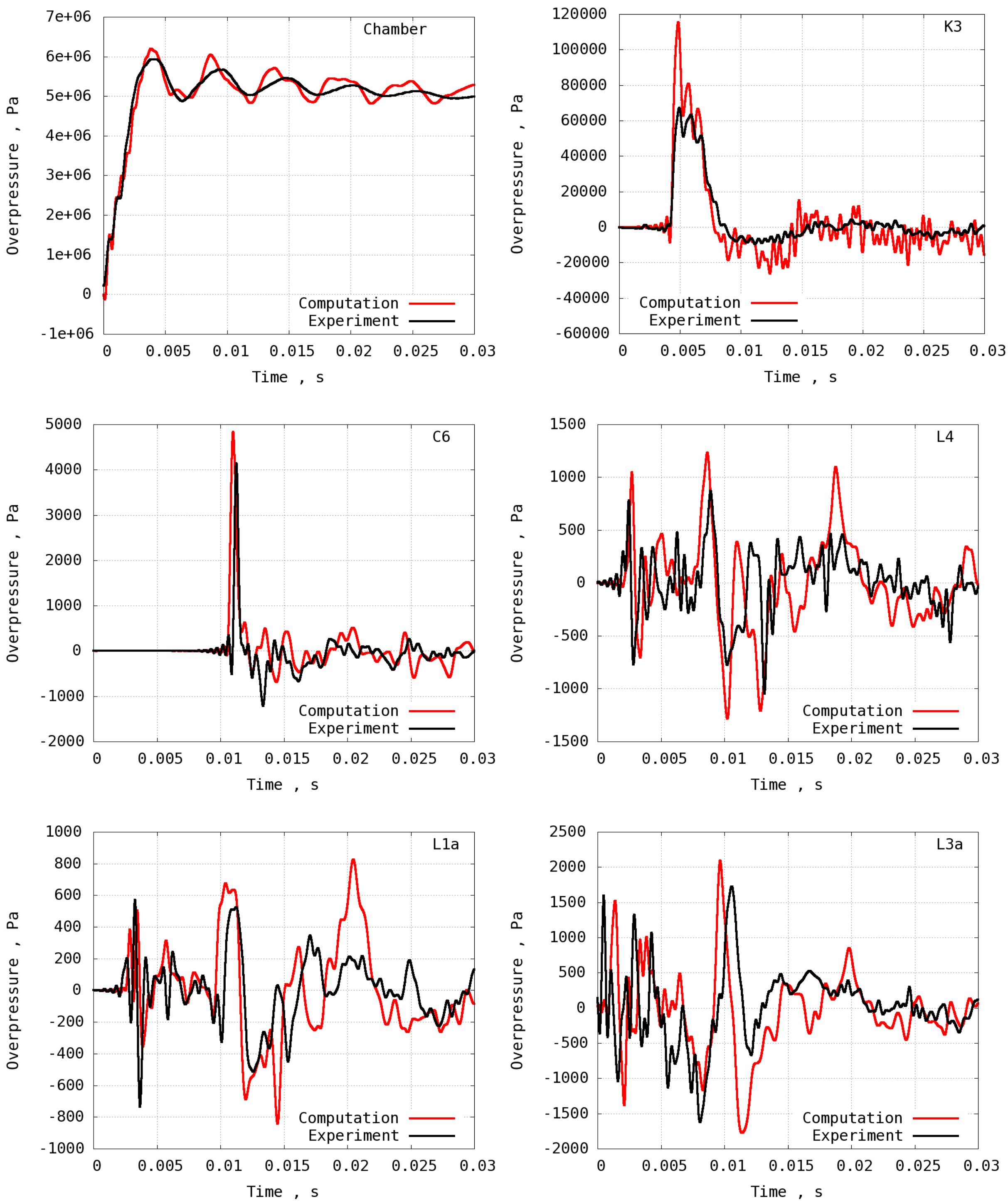

Figure 9: Pressure histories for the CEDRE computation and the Martel experiment

Inside the secondary chamber, results are in good agreement with the experiment. The pressure rise rate, which generates the overpressure wave, is correctly recreated. The propagation of the pressure wave inside the flame trench can be seen on the Figure 9 (sensor K3). While the moment of the DOP emergence is accurately computed, its magnitude is overestimated in the trench.

Outside the trench (sensors C6 and L4), the computed histories are in agreement with the experiment, despite a 0.25 ms temporal advance over the experimental reference for sensor C6. That advance could be related to a doubt about the experimental sensor location.

The generator sensors (L1a and L3a) are the most important locations of measuring, as they can be directly linked to the loads applied on the launcher. Although the IOP can be underestimated (sensor L1a) and the DOP overestimated (sensor L3a), the results seem to be in agreement, which infers that the computation has correctly reproduced the experimental wave generation. Besides, some sensors (L4, L1a) show a secondary pressure peak occurring 10 ms after the DOP. Such a peak will be studied thoroughly in the next part.

The pressures histories were previously compared to an experimental pressure averaged. Such an approach will be completed by a comparison to the array of reference gusts.
For each sensor, and for each reference gust, the peak to peak amplitude of the IOP and the DOP is noted. For each sensor, the most and the least powerful (depending on the gust) peak to peak amplitudes are drawn for the IOP (Figure 10) and the DOP (Figure 11). The IOP and DOP amplitudes of the computation are also drawn on the figures.

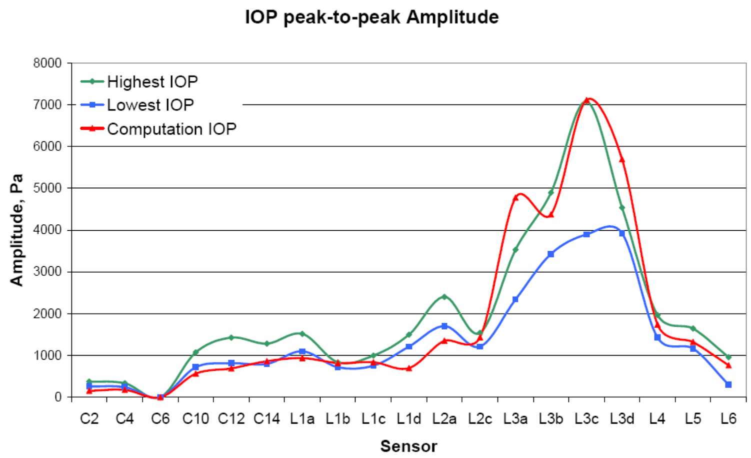

Figure 10: Peak-to-peak amplitude for the IOP

For most sensors, the IOP amplitudes seem slightly underestimated by the computation, which could be linked to the IOP crossing the complex geometry top-case, with multiples holes and edges. The results are nevertheless acceptable, as they approach the minimal IOP recorded at a reference Martel gust (blue curve, figure 10).

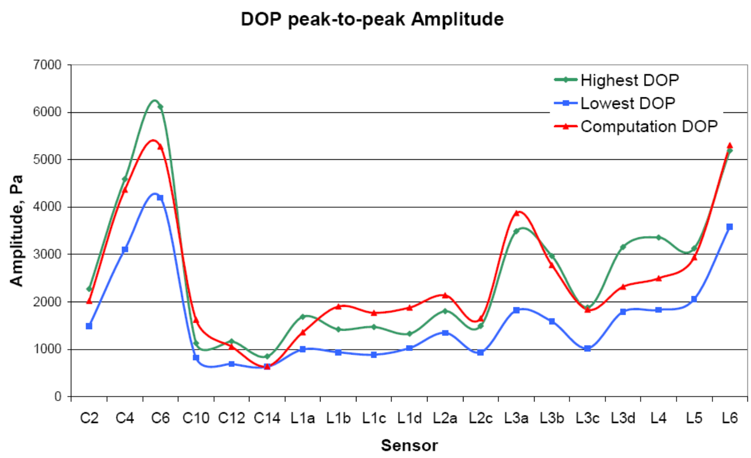

Figure 11: Peak-to-peak amplitude for the DOP

The agreement for the DOP results is fairly acceptable for most sensors (Figure 11), except for sensors L1a to L2a where the DOP is overestimated. Such an overestimation near the generator could be explained by a combination between the DOP coming from the trench exit towards the generator and the IOP exiting through the top case.

As a conclusion, despite the bias on some sensors, the computation run can be considered valid, and will therefore be used to the pressure observations.

4.3 Observation of the results

4.3.1 Emission of the pressure waves

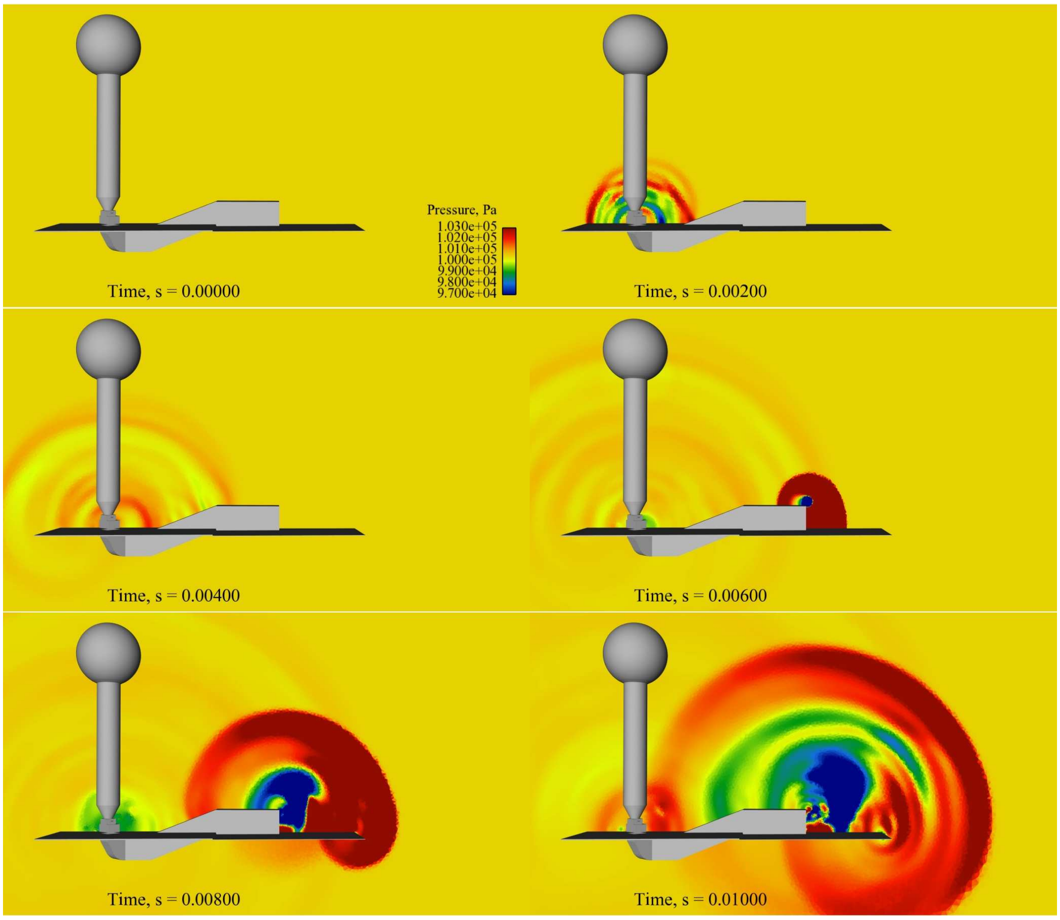

Figure 12: Peak-to-peak amplitude for the DOP

Figure 12 shows the evolution of the pressure on a vertical plane crossing the trench. Both the IOP and the DOP are distinguished. The IOP exits through the top case located on top of the trench, while the DOP is generated at the exit of the trench and propagates back to the generator. For every sensor except C6, the IOP precedes the DOP, which tallies with the pressure histories studied in part 4.2. Besides, a combination between the IOP and the DOP can be seen on the Figure 12 at 10 ms. That combination raises the bias between the simulated and measured DOP, and could be the main cause of the overestimation on sensors L1a to L2a.

4.3.2 Propagation inside the flame trench

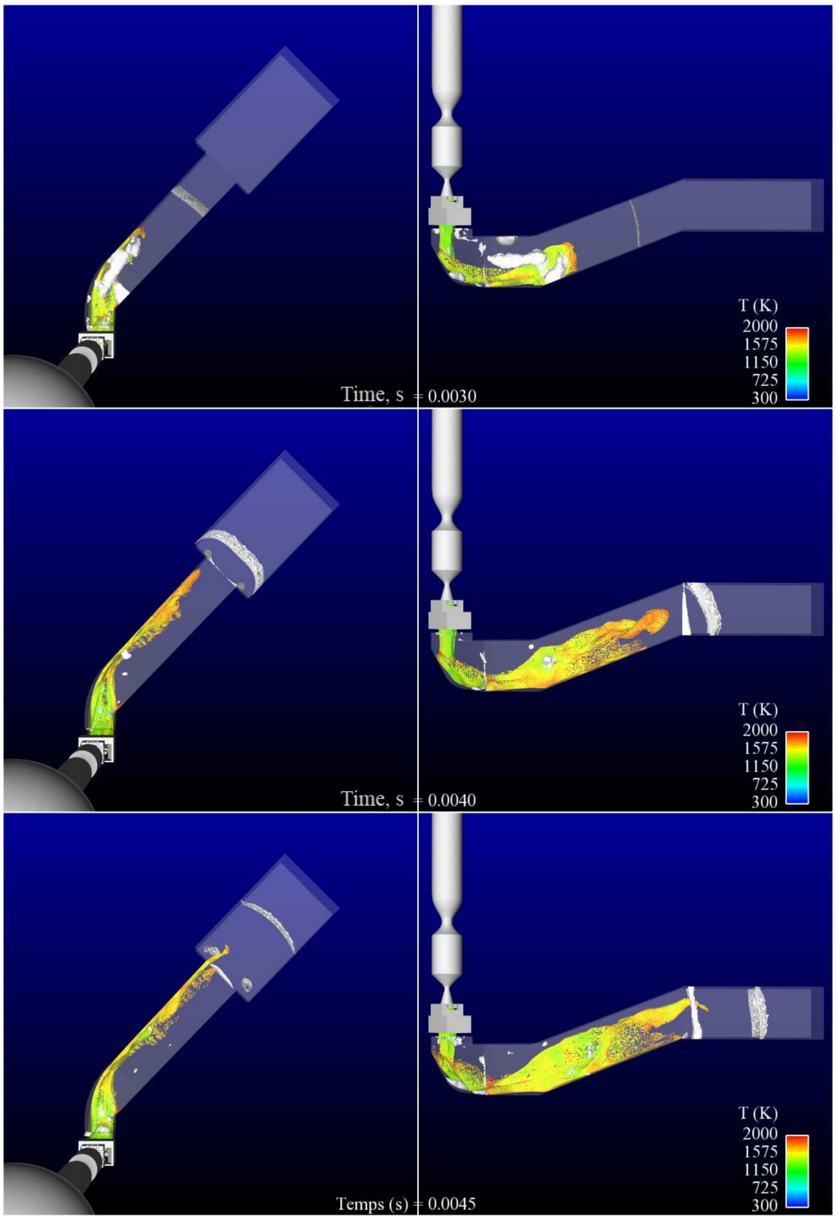

Figure 13: Plume flow (colored by temperature, products mass fraction isosurface) and overpressure wave (white 101 kPa isosurface)

The trench used at Martel facility is similar to the Kourou launchpad at a reduced scale. Its geometry is complex, as it includes several curves and a section modification in its final part. Inside the flame trench, the pressure wave is clearly ahead of the plume flow (Figure 13).

Moreover, the observation of the propagation of the pressure wave and the plume flow in the trench underlines the fact that the successive curvatures of the flame trench have no influence on the wave front, which remains plane after each bend. On the other hand, the plume is shaped by the trench geometry and occupies the bottom left corner of the trench.

The section modification of the last part of the trench has no effect on the plume flow but turns the wave front to a spherical wave. That modification is progressively reverted in the final part of the trench, before the exit.

4.3.3 Study of the additional pressure peak

In the computation, an additional pressure peak can be seen on several sensors. Its amplitude may vary and even exceed the DOP amplitude (sensor L1a, Figure 9). The pressure peak can be related to a generation of a second DOP at the trench exit between 15 and 16 ms of the simulation (cf Figure 14).

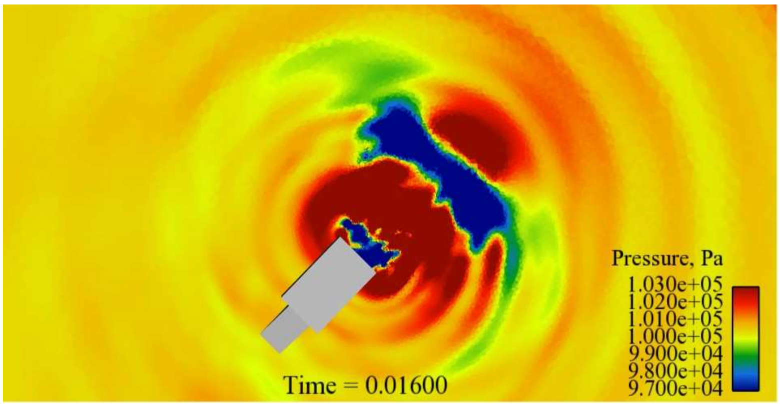

Figure 14: Generation of the additional pressure peak at 16 ms

During the blast, the flow reaches a steady state at 15 ms. Before that moment, the flow is in a transient state, and heavy pressure variations cross the trench, as it can be seen on Figure 15:

- the DOP enters the trench at 0.5 ms, propagates into the duct, and crosses its exit at 5.25 ms
- between 5.5 and 6 ms, a low pressure zone appears at the trench exit and propagates back to the entry
- at last, the additional pressure peak is formed between 15.5 and 16 ms at the trench exit

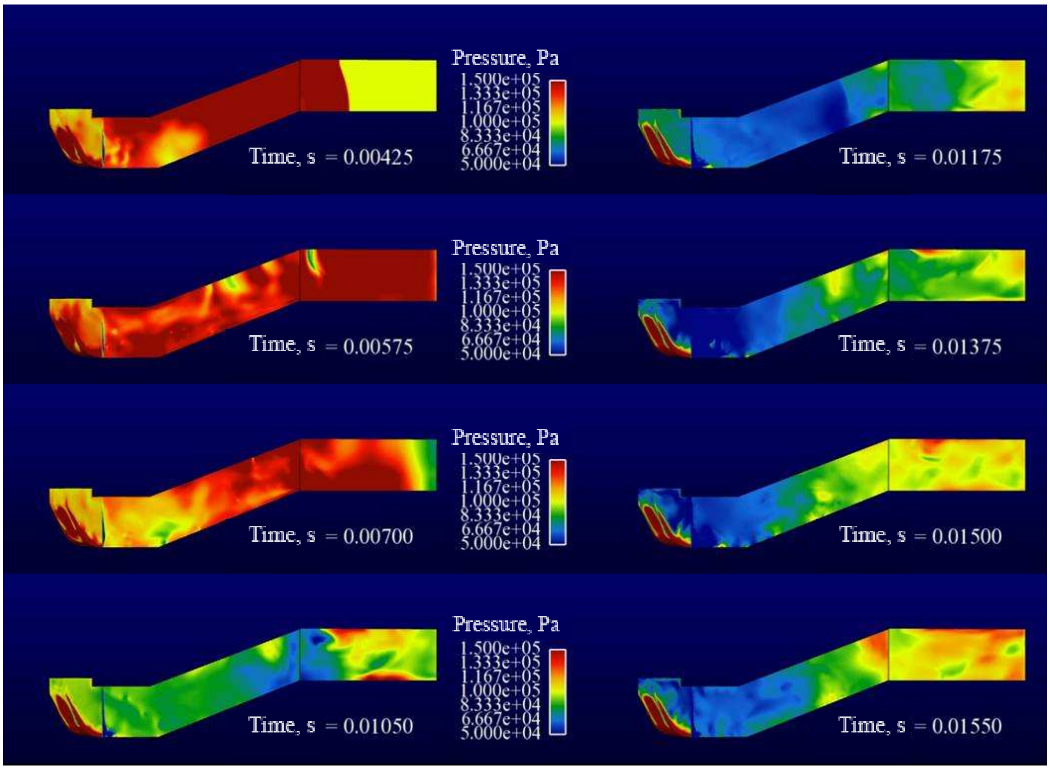

Figure 15: Pressure on the trench walls

The additional pressure peak is therefore related to the acoustic response of the trench. The response depends on the trench geometry and is not visible on the Martel experiment with such great amplitude.

5. Conclusion

The computation carried out was part of the first numerical study of the pressure wave generation at the Martel facility and needed a combustion computation in order to determine the chemical and thermodynamical properties of the burnt gases.
Wave generation results proved to be in agreement with the Martel experiment, and were subsequently used in order to explain the phenomena involved in the wave pressure generation and propagation.
As a conclusion, the detailed pressure wave numerical simulation will be used as a touchstone in order carry out several modified computations. Those computations will rely on geometric modifications or water injection systems to infer their influence on the pressure wave mitigation.

Acknowledgements

The authors would like to acknowledge teams from CNES for their support, from Astrium-ST for the generator geometry, and from CEAT and Onera for their help regarding the experiment.

References

[1] H. Ikawa and F.S. Laspesa. 1982. *Space shuttle SRM ignition overpressure prediction methodology. 13th Plume Technology Meeting*. Houston, Texas.
[2] J. Varnier. 2005. Experimental study of the blast wave ignition of rocket engines. 6th International Symposium on Launchers technologies. Munich.
[3] D. Gély, J-C. Valière, H. Lambaré, H. Foulon. 2006. Overview of aeroacoustic research activities in MARTEL facility applied to jet noise. *Internoise 2006 - 35th International Congress and Exposition on Noise Control Engineering.*
[4] C. Bresson, H. Foulon, H. Lambaré, M. Poleet, P. Malbéqui. 2010. A blast wave generator in MARTEL facility to simulate overpressure induced by solid rocket motor at lift-off. *4th European Conference for Aerospace Sciences, EUCASS*, 4-8 July, Saint-Petersburg.
[5] J. Troyes, F. Vuillot, J. Varnier, P. Malbéqui. 2009. Numerical simulations of rocket solid motor engine ignition and duct overpressure waves at reduced scale. *45th AIAA/ASME/SAE/ASEE Joint Propulsion Conference & Exhibit, Denver, Colorado.*
[6] J.-B Dargaud, J. Troyes, F. Vuillot, C. Bailly. 2010. Numerical simulations of model solid rocket motor ignition overpressure waves. Part I: horizontal free jet with ground. *ICVS17*, Cairo, Egypt.
[7] J. Troyes, F. Vuillot, J.-B Dargaud. 2010. Numerical simulations of model solid rocket motor ignition overpressure waves. Part II: vertical firing with flame duct. *ICVS17*, Cairo, Egypt.
[8] P. Chevalier et al. 2005. CEDRE: Development and validation of a multiphysic computational software. *1st European Conference for AeroSpace Sciences*. Moscow.
[9] G. Boudier. 2006. Methane/Air flame with 2-step chemistry: 2S-CH4-CM2, private communication, QPF CERFACS, 7.2.